

This is an Open Access document downloaded from ORCA, Cardiff University's institutional repository: <https://orca.cardiff.ac.uk/id/eprint/123721/>

This is the author's version of a work that was submitted to / accepted for publication.

Citation for final published version:

Zheng, Shuang, Lourenço, Sérgio D.N., Cleall, Peter J. and Ng, Angel K.Y. 2019. Erodibility of synthetic water repellent granular materials: adapting the ground to weather extremes. *Science of the Total Environment* 689 , pp. 298-412. 10.1016/j.scitotenv.2019.06.328

Publishers page: <https://doi.org/10.1016/j.scitotenv.2019.06.328>

Please note:

Changes made as a result of publishing processes such as copy-editing, formatting and page numbers may not be reflected in this version. For the definitive version of this publication, please refer to the published source. You are advised to consult the publisher's version if you wish to cite this paper.

This version is being made available in accordance with publisher policies. See <http://orca.cf.ac.uk/policies.html> for usage policies. Copyright and moral rights for publications made available in ORCA are retained by the copyright holders.



Erodibility of synthetic water repellent granular materials: adapting the ground to weather extremes

Shuang Zheng¹, Sérgio D.N. Lourenço^{1*}, Peter J. Cleall², Angel K.Y. Ng³

¹ Department of Civil Engineering, The University of Hong Kong, Hong Kong S.A.R., China

² School of Engineering, Cardiff University, United Kingdom

³ Ove Arup & Partners (Hong Kong) Ltd., Hong Kong S.A.R, China

* Corresponding author

1
2
3
4
5
6
7
8
9
10
11
12
13
14
15
16
17
18
19
20
21
22
23
24
25
26
27
28
29
30
31
32
33
34
35
36
37
38
39
40
41
42
43
44
45
46
47
48
49
50
51
52
53
54
55
56
57
58
59
60
61
62
63
64
65

1 **Abstract**

2

3 Granular materials with synthetic water repellent coatings have great potential to be
4 used in ground interfaces (ground-atmosphere-vegetation and ground-structure) as
5 infiltration barriers, due to their altered hydrological properties (suppressed infiltration
6 and decreased sorptivity). However, very few studies have evaluated the impact of
7 synthetic soil water repellency on soil erosion. This paper investigates the effect of
8 water repellency on soil erosional behavior, including splash erosion and rill
9 processes. Twenty-four flume tests were carried out on model slopes under artificial
10 rainfall; soils with three wettability levels were tested, including wettable (contact
11 angle, $CA < 90^\circ$), subcritical water repellent ($CA \sim 90^\circ$) and water repellent ($CA > 90^\circ$).
12 Various rainfall intensities (230 mm/h, 170 mm/h, 100 mm/h and 40 mm/h) and grain
13 sizes (Fujian sand and sand/silt mixture) were adopted. Erosional variables, including
14 splash erosion rate, average sediment concentration, peak sediment concentration
15 and time to peak sediment were measured to quantitatively analyze the behavior. This
16 study confirms the impact of water repellency on soil erosion and unveils the
17 possibility to reduce infiltration at ground-atmosphere interface with controlled soil
18 erosion. The results revealed that: (1) synthetic water repellency does not necessarily
19 lead to increased soil erosion yield; its impact is dependent on grain size with the soil
20 erosion loss increasing for Fujian sand, but decreasing for sand/silt mixtures; (2)
21 splash erosion is positively correlated to soil water repellency and high rainfall
22 intensity, regardless of grain size; (3) the erosion processes for sand/silt mixtures are

23 particle size selective and not affected by soil water repellency, whereas this
24 phenomenon is not observed with Fujian sand.

25

26 **Keywords:** Synthetic soil water repellency, flume test, soil erosion, splash erosion,
27 particle size selectivity

28 **1. Introduction**

29

30 The influence of soil water repellency on the soil hydrological behavior has been
31 extensively investigated, both in the natural environment and the laboratory (Mao et
32 al., 2019). It is known to increase the water entry value (Wang et al., 2000), decrease
33 the infiltration capacity (Doerr et al., 2006), sorptivity (Ebel and Moody, 2017), field
34 saturated hydraulic conductivity (Fox et al., 2007) and therefore lead to promoted
35 overland flow (Jordán et al., 2016). The distinctive hydrological properties of synthetic
36 water repellent soils suggest that it may be utilized in the built environment, as
37 infiltration barriers, for slope stabilization or ground improvement measures (Lourenço
38 et al., 2018; Dell'Avanzi et al., 2010). As an important component of land degradation,
39 soil erosion was observed to increase considerably on naturally occurring water
40 repellent soils (Doerr et al., 2006), due to reduced infiltration and enhanced overland
41 flow (Cerdà et al., 1998), promoted rain splash detachment of soil (Shakesby et al.,
42 1993) and increased soil erodibility (Sheridan et al., 2007). Nevertheless, little exists
43 on the impacts of synthetic soil water repellency on soil erosion (Mohammadi et al.,
44 2018). For instance, synthetic soil water repellency is induced by films with a
45 thickness in the μm range (up to $10\ \mu\text{m}$) and with physical properties that differ from
46 natural water repellent substances. The coatings are soft and smoothen the particle
47 surface (Liu et al., 2019). Therefore, an insight is needed on the erosional behavior of
48 soils with synthetic water repellent coatings.

49

50 Previous research mainly focused on the interaction between raindrops and water
51 repellent soils on small samples. Terry and Shakesby (1993) conducted a series of
52 simulated rainfall experiments and concluded that rain splash detachment is more
53 prominent on water repellent soil than on wettable soil. This influence of soil water
54 repellency, either naturally occurring or chemically induced, has been confirmed by
55 Ahn et al. (2013) and Jordán et al. (2016), revealing a greater splash distance, higher
56 ejecting velocity and larger splash erosion rate. In laboratory experiments in synthetic
57 water repellent sands, McHale et al. (2007) identified the formation of liquid marbles
58 as a mechanism which promotes erosion of loose water repellent sand: water droplets
59 which are fully covered by the soil particles and are highly mobile on sloping surfaces.
60 Atherton et al. (2016) assessed the interaction of water drops impacting multi-layered
61 bead packs with mixed soil wettability, and suggested that a water repellent top layer
62 can increase splash erosion without affecting the matrix below. Wettable particles just
63 below the surface, however, may result in multiple layers of the soil matrix eroding
64 simultaneously. Despite past research on rain splash erosion, questions remain on
65 the erosional impacts of soil water repellency, including different erosional processes
66 (rill and splash erosion) and at scales greater than the previous studies.

67

68 To comprehensively assess the overall erosional impacts of soil water repellency, it is
69 vital to separate the different types of processes. Bryan (2000) identified two distinct
70 sub-processes of soil erosion in natural slopes: interrill and rill processes. Interrill
71 erosion includes the detachment of soil by rain splash and following entrainment by

72 shallow surface flow, this process is primarily dominated by the kinetic energy of rain
73 splash, which can be determined by the rainfall intensity and raindrop size distribution
74 (Carollo et al., 2017). A threshold kinetic energy, which is dependent on soil properties,
75 has to be reached for a raindrop to be erosive and initiate soil dislodgement (Greene
76 and Hairsine, 2004). Rill erosion is caused by concentrated flow and not directly
77 influenced by raindrop impact, where it depends on both the flow behavior (flow
78 velocity, turbulence level etc.) and the soil's resistance to concentrated flow.

79

80 Rainfall is one of the major active agents of soil erosion, its capability to erode soil, i.e.
81 rainfall erosivity is closely related to the rainfall characteristics (rainfall intensity,
82 duration, kinetic energy etc.) (van Dijk et al., 2002). In RUSLE (Revised Universal Soil
83 Loss Equation, Renard et al., 1991), rainfall erosivity is calculated by multiplying the
84 kinetic energy of the rainfall by the maximum continuous 30-min intensity in the event.
85 A soil's resistance to erosion, or soil erodibility is strongly dependent on soil properties,
86 including grain size, initial moisture content, shear strength, aggregate stability,
87 organic matter content, etc. (Knapen et al., 2007; Sheridan et al., 2000). Ayoubi et al.
88 (2018a) evaluated soil properties affecting soil loss in central Iran, indicating that soil
89 erodibility indices (runoff volume, soil loss, and sediment concentration) showed
90 positive and significant correlations with bulk density and negative correlations with
91 mean weight diameter, soil organic carbon, clay content and soil shear strength. The
92 spatial pattern of soil redistribution rate was explored using the Cs-137 technique
93 (Afshar et al., 2010; Ayoubi et al., 2012; Rahimi et al., 2013), demonstrating the

94 effects of human activities and land use on soil erosion.

95

96 This paper attempts to evaluate the erosional behavior of soils with artificially induced
97 water repellency, to facilitate the utilization of synthetic water repellent soils in the built
98 environment, by means of model granular materials and under laboratory-controlled
99 conditions. No roots, organic matter and vegetative ash were involved. The specific
100 objectives of the study are: (1) to evaluate the influence of water repellency on splash
101 erosion and the initiation of rill erosion; (2) to investigate the interaction effect between
102 water repellency and grain size on soil erosion, and (3) to elucidate the different
103 mechanisms involved.

104

105 **2. Materials and Methods**

106

107 *2.1. Soil description*

108

109 As sands are cohesionless and easily erodible granular materials, and soil erodibility
110 was reported to decrease with the decrease in silt fraction (Wischmeier and
111 Mannering, 1969), two model (or mineral) soils with different grain size distributions
112 are adopted in this paper: Fujian sand (China ISO standard sand) and crushed silica
113 (silt). The erosional behavior of these two soils are expected to be different. Fujian
114 sand is a clean, siliceous sand consisting preferably of rounded particles with a silica
115 content $\geq 98\%$. Its particle size distribution complies with ISO 679:2009, as displayed

116 in Fig. S1, and is classified as poorly graded sand. Crushed silica has the same
117 composition as Fujian sand, and is crushed with a median size of 20 μm (silt). The
118 grain size distribution of crushed silica is obtained using a particle size and shape
119 analyzer (QICPIC, Sympatec GmbH, Germany) and presented in Fig. S1 as well. The
120 physical properties of Fujian sand and crushed silica are summarized in Table 1. The
121 specific gravity, coefficient of uniformity and coefficient of curvature were determined
122 following BS 1377-2 (British Standards Institution, 1990). The organic matter content
123 was determined via loss on ignition (LOI) analysis (BS 1377-3), by heating the
124 sub-samples at 450 °C for 1 hour. The maximum void ratio and minimum void ratio
125 were determined by following the procedures in BS 1377-4.

126

127 *2.2. Soil silanization*

128

129 The occurrence of soil water repellency normally results from the presence of water
130 repellent coatings around the soil particles. Dimethyldichlorosilane (DMDCS) has
131 been widely used in previous studies (Bachmann et al., 2000; Ng and Lourenço, 2016)
132 as a hydrophobizing agent to artificially induce water repellency in soil samples. The
133 treatment is based on silanization, by reaction between DMDCS and residual water,
134 polydimethylsiloxane (PDMS) is formed and bonded to the soil particle surface along
135 with the formation of HCl gas as a by-product. The level of water repellency is
136 dependent on the DMDCS concentration and soil type. Zheng et al. (2017) treated the
137 natural completely decomposed granite with 3% of DMDCS by soil mass to attain a

138 CA of 115°. Ng and Lourenço (2016) found that the maximum CA can be induced
139 using 3% and 0.005% DMDCS by soil mass for alluvium and Leighton Buzzard sand,
140 respectively. For Fujian sand and crushed silica, the critical DMDCS concentrations to
141 reach the maximum CA are 0.1% and 0.2% respectively, as indicated by Fig. S2. To
142 allow soil water repellency to establish and for consistency among the tests, the
143 materials were treated and equilibrated at ambient air conditions for 3 days before
144 using.

145

146 2.3. *Soil water repellency assessment*

147

148 Materials of various water repellency levels were used in this study, and the water
149 repellency level of soil samples was assessed with two measuring techniques: sessile
150 drop method (SDM) and water drop penetration time (WDPT).

151

152 The SDM is a direct method to measure the CA of water drop on a soil sample surface
153 (Bachmann et al., 2000). When a drop of water is dispensed on a surface, the
154 three-phase contact line between the soil, water, and air will move in response to the
155 three interfacial tensions, forming a CA which is a direct quantification of soil
156 wettability. The CA of a wettable soil and water repellent soil is $< 90^\circ$ and $> 90^\circ$
157 respectively, and a subcritical water repellent soil has a CA $\sim 90^\circ$, which is generally
158 regarded as a wettability boundary between wettable and water repellent conditions.

159 The CA measurement procedures were introduced by Bachmann et al. (2000) and

160 improved by Saulick et al (2017) as follows: (1) the soil is sprinkled on a double-sided
161 adhesive tape fixed on a glass slide, and by removing the excess particles to ensure a
162 monolayer of particles is fixed; (2) placing the slide on a goniometer's (DSA 25,
163 KRÜSS GmbH, Germany) sample stage and dispensing a droplet of deionized water
164 (10 μ L) onto the sample; (3) contact angle measurements are then performed by
165 analyzing the shape of the droplet on the soil surface. Six drops were applied to the
166 surface of each soil sample.

167

168 WDPT is an index test that evaluates the persistence of water repellency of a soil
169 sample (Doerr, 1998). The test is conducted by placing a drop of deionized water (50
170 μ L, same as in Leelamanie et al., 2008) on the surface of prepared soil sample and
171 recording the time taken for the water drop to completely infiltrate (Doerr, 1998). For
172 wettable soils, the water drop should penetrate within 5 s (Bisdom et al., 1993), and
173 for water repellent soils, the stronger the water repellency the longer the penetration
174 time. Based on the WDPT, the water repellency of soils can be classified into different
175 categories, from wettable to extremely water repellent. For each soil sample, the
176 WDPT of 6 drops were measured.

177

178 **3. Flume tests**

179

180 *3.1. Flume configuration*

181

182 Flume tests have been widely adopted to investigate the hydrological and geomorphic
183 behavior of various types of soils under artificial rainfall (Bryan and Poesen, 1989; Shi
184 et al., 2017). In this paper, a perspex-sided flume was manufactured to carry out the
185 experiments, and the dimensions of the slope model were 80 cm long, 40 cm wide
186 and 5 cm deep. To facilitate the collection of water and eroded sediment, a collection
187 system was installed at the downslope edge of the flume. Sandpaper (Simax
188 LPE-22-4) was glued on the base of the flume to provide friction, and a permeable
189 baffle was installed at the toe to prevent the model slope from sliding at the soil-flume
190 interface, while water was allowed to drain through. A rainfall simulation system was
191 installed to generate the desired rainfall intensities (40, 100, 170 and 230 mm/h). The
192 system consisted of a nozzle (FullJet, Spraying Systems, US), a flowmeter and a
193 control valve to ensure constant rainfall intensity during tests. Two FDR (frequency
194 domain reflectometry) moisture sensors (EC-5, Decagon Devices, US) were buried at
195 the same depth (4 cm), one near the slope toe and the other near the crest to track
196 the wetting front movement. A video camera (HERO4 Silver, GoPro, US) was
197 positioned above the slope surface to record surface morphology evolution. Fig. 1
198 shows the configuration of the flume and instrumentation.

199

200 3.2. *Model preparation and test procedures*

201

202 The model was filled with the dry soil in a horizontal orientation (i.e. slope angle of
203 zero) into 5 layers with a thickness of 1 cm, no compaction was applied to make sure

204 the soils were in loose state and readily erodible, with the minimum bulk density of
205 1.77 g/cm^3 achieved. The slope surface was smoothed by a wooden block to help
206 eliminate differences in surface conditions among experiments, then the flume was
207 inclined to a slope angle of 10° .

208

209 The data logger, camera and stopwatch were synchronized before the experiments
210 began and started recording once the rainfall simulator was activated. Each
211 experiment lasted for 120 minutes, as preliminary testing indicated that the steady
212 state condition was achieved within 120 minutes. The wetting behavior or spatial
213 evolution of water content was traced by the FDR moisture sensors. The runoff and
214 eroding sediment were collected by a container at the slope toe at 5-min intervals
215 (2-min intervals for high rainfall intensities). In this study, the term “runoff” not only
216 implies overland flow but also includes subsurface flow that eventually flows out of the
217 flume (for wettable soils). In this context, the runoff is equivalent to the difference
218 between rainfall intensity and water stored in soil mass and equals to the rainfall
219 intensity when the steady state (near-saturation) is reached. After the rainfall event,
220 the collected sediment was oven dried to determine the mass of water, sand and silt
221 (if present) for further analysis. Particle size distribution analysis was carried out for
222 samples obtained at each collecting interval.

223

224 *3.3. Testing program*

225

226 To investigate the influence of soil wettability, grain size and rainfall intensity on soil
227 erosion, a factorial design of flume tests involving these three factors was used in this
228 study. A total of 24 flume tests were conducted and are listed in Table 2. Four rainfall
229 intensities (40, 100, 170 and 230 mm/h) were selected to cover a wide range of
230 rainfall scenarios, the exceptional ones were adopted to compensate for the influence
231 of smaller raindrop velocity and achieve a high enough kinetic energy. Two different
232 grain sizes: Fujian sand and 50/50 sand/silt mixture (silt is crushed silica) were
233 selected, to examine the effect of grain size on soil erosion under wettable and water
234 repellent conditions. The tests were not repeated, as the model materials were
235 adopted, with the initial condition (e.g. dry density, slope angle etc.) well controlled, all
236 sensors and nozzles were calibrated before conducting experiments.

237

238 Following Zheng et al. (2017), three water repellency levels were selected based on
239 the CA and WDPT achieved. For wettable soils, no treatment was applied and the CA
240 and WDPT were lowest (CA = $20.3 \pm 2.6^\circ$ for Fujian sand and $71.1 \pm 5.3^\circ$ for crushed
241 silica; WDPT = 0 s). The different CAs between Fujian sand and crushed silica was a
242 result of changing particle size, as the CA increased with decreased particle size
243 (Saulick et al., 2018). The critical DMDCS concentrations were used for the treatment
244 of water repellent soils, i.e. 0.1% and 0.2% for Fujian sand and crushed silica
245 respectively, with the maximum CA and WDPT > 3600 s attained (Fig. S2). For
246 subcritical water repellent conditions, the concentrations of DMDCS adopted for
247 Fujian sand and crushed silica were 0.05% and 0.1%, respectively, with the CA of ~

248 90° achieved.

249

250 3.4. *Soil splash test*

251

252 To determine the soil splash erosion rate, 24 soil splash tests were carried out under
253 the same conditions as the flume tests (rainfall intensity, CA and grain size). A similar
254 set-up as in Jordán et al. (2016) was adopted. For each test, six splash cups (5.5 cm
255 radius) filled with dry soil were prepared and the mass weighed. Then the cups were
256 placed under the spraying nozzle and subjected to 30-min rainfall at the designated
257 rainfall intensity, subsequently, the remaining soil was oven dried and weighed to
258 determine the splash erosion rate.

259

260 3.5. *Data analysis*

261

262 To quantitatively analyze the raw data obtained from the tests, a series of variables
263 were defined as follows:

264

- 265 • Splash erosion rate (E_s , g/mm): The mass of soil splash loss divided by the
266 rainfall depth (as defined in Terry and Shakesby, 1993);
- 267 • Average sediment concentration (S_a , g/L): Total mass of sediment in runoff
268 divided by the total volume of runoff throughout the experiment; total mass of
269 sediment is also calculated and plotted as a reference (as defined in Asadi et

270 al., 2011);

271 • Peak sediment concentration (S_p , g/L): The maximum sediment concentration
272 in a 5-min interval (2-min for high rainfall intensity conditions);

273 • Time to peak sediment (T_p , minute): The time when maximum sediment
274 concentration is recorded; time to peak runoff is also recorded and plotted as a
275 reference.

276

277 3.6. *Statistical analysis*

278

279 Statistical analyses were performed using Real Statistics Resource Pack software
280 (Release 5.4, Zaiontz, 2018) and MATLAB (R2014b, MathWorks, US). A factorial
281 analysis of variance (ANOVA) followed by a Tukey's HSD test was conducted to
282 examine statistically significant differences (level of significance = 0.05) in the values
283 of variables from different experiments. Regression analysis (Tajik et al., 2012;
284 Ayoubi et al., 2018b) was adopted to characterize the relationships between rainfall
285 intensity, CA and soil erosion variables. The best-fitting equations all 4 variables were
286 presented for Fujian sand and sand/silt mixture separately. A correlation matrix of the
287 Pearson correlation coefficients was obtained to analyze the correlations between
288 rainfall intensity, wettability level and soil erosional parameters (level of significance =
289 0.05).

290

291 **4. Results**

292

293 To describe the typical hydrological and erosional responses, the time series data
294 were analyzed and presented, including runoff rate, sediment concentration,
295 volumetric water content and surface morphology. Based on the wettability level and
296 grain size, the tests were classified into 5 groups, i.e. (1) wettable and subcritical
297 water repellent sand, (2) water repellent sand, (3) wettable sand/silt mixture, (4)
298 subcritical water repellent sand/silt mixture and (5) water repellent sand/silt mixture.
299 Due to large number of tests, five tests (one from each group) were analyzed and
300 presented in Fig. 2-6. The soil erosional variables of each test were summarized in
301 Table 2 and Fig. 7, where the time to peak sediment, average sediment concentration,
302 peak sediment concentration, total mass of sediment and time to peak runoff of Fujian
303 sand and sand/silt mixture were presented separately, due to the contrasting behavior
304 between the two grain sizes. In addition, Fig. 8-9 compared the results among tests
305 and examine the impacts of grain size, rainfall intensity and soil wettability. The splash
306 erosion rate and the sediment particle size distribution analysis were shown in Fig. 8
307 and Fig. 9, respectively.

308

309 *4.1. Temporal evolution of erosion*

310

311 *4.1.1. Wettable and subcritical water repellent sand*

312

313 Test 7 (Fujian sand, CA = 20°, rainfall intensity = 170 mm/h) shows the typical
314 hydrological and erosional responses, with the results presented in Fig. 2. At the
315 rainfall onset, all rainwater infiltrated and no surface runoff was observed (Fig. 2a).
316 The wetting front was parallel to the surface and the moisture sensor readings
317 remained unchanged (Fig. 2b). At 2 min, a sudden rise in volumetric water content
318 was recorded by both sensors 1 and 2, implying that the wetting front had reached the
319 sensors (4 cm deep). Subsequently, a jump in runoff rate occurred at 4 min until a
320 steady state was reached at 8 min (Fig. 2a), i.e. all rainwater converted into runoff with
321 the runoff rate becoming equal to the rainfall intensity. The volumetric water content
322 increased to 28.5% at steady state (Fig. 2b), with the volumetric water content at
323 saturation was 34.5%.

324

325 As for the soil erosional behavior, the sediment concentration at each sampling
326 interval was calculated. The sediment concentration experienced a drop (from 6.7 to
327 0.6 g/L) after the test began, which was a result of the substantially increased runoff
328 rate (from 3.4 to 177.8 mm/h), although the sediment mass barely changed at this
329 stage. After the steady state was reached, the entrainment and transportation of
330 particles by surface runoff dominated the erosional processes. With the development
331 of surface flow and rill erosion (Fig. 2c), the erosivity of the concentrated flow in the
332 rills increased and subsequently the sediment concentration started to show a sharp
333 rise until the peak sediment concentration was recorded at 20 min. For wettable and
334 subcritical water repellent sand, the increase in rainfall intensity led to decreased time

335 to peak sediment (Fig. 7a), whereas the average sediment concentration (Fig. 7c) and
336 peak sediment concentration (Fig. 7e) were positively influenced by rainfall intensity.
337 The time to peak sediment was shortened from 120 min (under 40 mm/h rainfall) to 15
338 min (under 230 mm/h rainfall). The average sediment concentration was 0.0 g/L at the
339 rainfall intensity of 40 mm/h, implying that a higher rainfall intensity was necessary to
340 initiate erosion, while the average sediment concentration and peak sediment
341 concentration under 230 mm/h rainfall were 47.75 g/L and 89.67 g/L, respectively.

342

343 4.1.2. Water repellent sand

344

345 The results of test 3 (Fujian sand, $CA = 120^\circ$, rainfall intensity = 230 mm/h) were
346 presented in Fig. 3. Infiltration was suppressed regardless of the rainfall intensity, with
347 the steady state runoff achieved at the beginning of test (Fig. 3a). The volumetric
348 water content remained constant throughout the test (Fig. 3b), indicating that no
349 infiltration occurred, an observation that is supported by the measured runoff rate.

350

351 As a result of enhanced overland flow, concentrated flow-driven soil erosion increased
352 substantially. The peak sediment (236.2 g/L) was recorded at the commencement of
353 the rainfall event, followed by a gradual decrease until reaching an approximately
354 constant level (45 g/L), which was greater than that of the wettable and subcritical
355 water repellent soil. Besides increased soil erosion, the surface morphology of water
356 repellent sand showed unique characteristics during the test. At the onset of the test,

357 erosion processes were dominated by rainsplash, as the sand particles were dry,
358 loose and readily detachable. Due to the presence of water repellency, the infiltration
359 of rainwater was suppressed with surface runoff appeared promptly. The sand
360 particles were then entrained by the downward surface runoff, causing localized
361 erosion, which formed a series of “steps” or cascades on the surface, as recorded in
362 Fig. 3c. As the erosion processes continued, the eroded zones expanded and merged,
363 with three major rills formed. The positive impacts of rainfall intensity on the erosional
364 variables of water repellent sand were revealed by Fig. 7. Higher rainfall intensity
365 resulted in reduced time to peak sediment (from 60 min to 5 min, Fig. 7a), as well as
366 increased average sediment concentration (from 2.25 g/L to 94.8 g/L, Fig. 7c) and
367 peak sediment concentration (from 3.57 g/L to 236.19 g/L, Fig. 7e), when the rainfall
368 intensity increased from 40 mm/h to 230 mm/h.

369

370 4.1.3. Wettable sand/silt mixture

371

372 The results of representative wettable sand/silt mixture are shown in Fig. 4 (test 16:
373 mixture, CA = 20°, rainfall intensity = 100 mm/h). The steady state was reached at 20
374 min, with the soil in a near saturation state (degree of saturation 90%). The sediment
375 concentrations of sand and silt experienced similar changes (Fig. 4a), no erosion was
376 recorded during the first 5 min of the experiment. At 10 min, a sudden rise in
377 volumetric water content was simultaneously recorded by sensor 1 and 2 (Fig. 4b).
378 Accompanied by the sharp increase in water content and runoff at 10 min,

379 concomitant growth in sand and silt sediment concentration was recorded, which
380 reached the peak sediment concentration (139.6 g/L for silt and 121.5 g/L for sand) at
381 20 min. Similar to other experiments, the sediment concentration reduced after the
382 peak till the end of the test. Cracks appeared within the first 5 min of a rainfall event,
383 as illustrated in Fig. 4c, which is a unique surface morphology characteristic that was
384 not observed in other conditions. It is assumed that the cracks may result from
385 localized variations in stress and strain conditions, and subsequent developments of
386 tensile stresses that lead to crack initiation. After the formation of cracks in the soil
387 surface, sand and silt particles were dislodged from the cracks and micro rills
388 developed. Owing to the imposed boundary conditions, surface runoff concentrated
389 on the sides of the flume and two major rills were formed at these locations within 20
390 min. Within the group of wettable sand/silt mixture tests (Fig. 7), the average sediment
391 concentration decreased from 83.49 g/L (40 mm/h) to 74.05 g/L (230 mm/h) (Fig. 7d)
392 and the peak sediment concentration dropped from 302.95 g/L (40 mm/h) to 160.81
393 g/L (230 mm/h) (Fig. 7f). The decreased sediment concentration does not imply less
394 soil erosion, but the increase in runoff was greater than the increase in erosion.

395

396 4.1.4. Subcritical water repellent sand/silt mixture

397

398 As can be seen in Fig. 5a, and unlike the subcritical water repellent sand test,
399 infiltration of rainwater was impeded in test 23 (mixture, CA = 90°, rainfall intensity =
400 40 mm/h). Preferential flow, instead of a parallel wetting front, was observed. The

401 readings of sensor 1 and 2 remained unchanged at the beginning until 30 min (Fig.
402 5b), implying the preferential flow reached the sensors. Development of runoff was
403 initially delayed and then followed by a sharp increase at 5 min and then a gradual
404 increase with steady state reached after 65 min. At the end of the test (after 120 min),
405 the degree of saturation was only 57%. The sediment concentration was 0.0 g/L for
406 sand throughout the test, whereas eroded silt particles had a peak sediment
407 concentration of 17.9 g/L, suggesting that higher rainfall intensity is needed to initiate
408 the erosion of sand particles, owing to greater particle mass.

409

410 Due to the relatively low rainfall intensity and sediment concentration of test 23 (40
411 mm/h), negligible change in surface morphology was observed. Therefore, test 5 (230
412 mm/h) was selected and four photos showing the surface morphology change were
413 exhibited in Fig. 5c. Unlike the wettable condition, no cracks were observed on the soil
414 surface. Rainsplash induced circular depressions appeared after the experiment
415 began, along with the development of surface runoff, the circular depression gradually
416 expanded and evolved into rills. It is worth noting that the surface became rougher on
417 eyesight with time, as a result of unequal erosion severity of coarse and fine particles.
418 The fine particles were easily eroded while the coarse particles remained, causing a
419 rougher surface at the end of the experiment. The increased rainfall intensity had
420 positive influence on erosional variables of subcritical water repellent sand/silt mixture
421 (Fig. 7). With the increase in rainfall intensity from 40 mm/h to 230 mm/h, the time to
422 peak sediment decreased from 15 min to 2 min (Fig. 7b), whereas the average

423 sediment concentration grew from 6.37 g/L to 28.45 g/L (Fig. 7d) and the peak
424 sediment concentration increased from 17.85 g/L to 89.01 g/L (Fig. 7f).

425

426 4.1.5. Water repellent sand/silt mixture

427

428 Test 6 (mixture, CA = 90°, rainfall intensity = 230 mm/h) was the representative test
429 and the results were presented in Fig. 6. Immediately after the onset of rainfall,
430 overland runoff appeared on the surface (Fig. 6a), in the form of liquid marbles, i.e.
431 water drops which rolled on the water repellent surface with a powder coating. No
432 infiltration occurred throughout the 120 min rainfall (Fig. 6b, unchanged readings of
433 sensor 1 and 2). Steady state was reached at 4 min, after a water film was formed on
434 the soil surface. At the same time, the maximum sediment concentration of sand and
435 silt grains was reached, with a sediment concentration of 32.4 g/L and 41.7 g/L
436 measured respectively (Fig. 6b). As the rainfall continued, localized erosion was
437 observed on the soil surface (“scars” in Fig. 6c). Subsequently, the dry soil beneath
438 was exposed to surface flow and eroded, with the eroded zones expanding till the end
439 of the experiment. When subjected to increased rainfall intensity (from 40 mm/h to
440 230 mm/h), the time to peak sediment was shortened from 15 min to 4 min (Fig. 7b),
441 whereas the average and peak sediment concentration increased from 6.58 g/L to
442 20.91 g/L (Fig. 7d) and from 20.22 g/L to 74.12 g/L (Fig. 7f), respectively.

443

444 4.2. *Soil splash erosion*

445

446 The splash erosion rate of all experiments was summarized in Fig. 8, the box and
447 whisker plots were adopted for clear comparison. The splash erosion rate increased
448 from wettable to subcritical water repellent to water repellent. However, the splash
449 erosion rates of water repellent soils had a greater standard deviation, indicating
450 potential variations in splash erosion severity at different locations. Rainfall intensity,
451 in comparison to soil water repellency, had a minor influence on soil splash erosion.
452 Within each wettability level, the splash erosion rate increased when subjected to
453 higher rainfall intensity, both for sand (Fig. 8a) and sand/silt mixture (Fig. 8b)
454 conditions. There was no significant difference observed between the mean splash
455 erosion rates of sand and sand/silt mixture, suggesting that splash erosion was not
456 sensitive to grain size change.

457

458 4.3. *Particle size distribution of eroded sediment*

459

460 To investigate the dynamic changes in sediment particle size distribution, analysis
461 was conducted with collected sediment at each time interval for each experiment.
462 Commonly used particle size distribution parameters were calculated, including D_{10}
463 (diameter of soil particles for which 10% of the particles are finer, similarly for D_{30} and
464 D_{60}), D_{30} , D_{60} , C_u (uniformity coefficient, defined as D_{60}/D_{10}) and C_c (coefficient of
465 curvature, defined as $D_{30}^2 / (D_{60} \times D_{10})$). All parameters showed similar trends and D_{60}

466 experienced the greatest change, therefore only the temporal evolution in D_{60} was
467 presented. Fig. 9a illustrated that the grain size distribution of eroding sediment for
468 sand barely changed with time, which was similar to the original soil throughout the
469 test, indicating that the erosion processes of sand were not size selective. A
470 representative test (test 3: Fujian sand, CA = 120°, rainfall intensity = 230 mm/h) was
471 highlighted to show the typical trend. On the contrary, a significant change in sediment
472 size distribution of sand/silt mixture was recorded (Fig. 9b). The D_{60} at the
473 commencement of experiments (0.063 mm) was much smaller than that of the original
474 soil (0.187 mm), followed by an increase until the D_{60} approximately equals to the
475 original value. A representative test (test 5: mixture, CA = 90°, rainfall intensity = 230
476 mm/h) was highlighted to show the typical trend. This dynamic change in sediment
477 size distribution suggests that the collected sediment at the early phase was
478 dominated by silt-sized particles. With the increased runoff rate, the transport of sand
479 particles was gradually activated, leading to a coarser sediment until the sediment
480 particle size distribution became similar to the original soil.

481

482 4.4. Regression analysis

483

484 For all obtained best-fitting equations, the independent variables (rainfall intensity and
485 CA) were normalized by its mean and standard deviation before curve fitting.
486 Therefore, the size of regression coefficients indicates the size of the effect that an
487 independent variable has on the dependent variable, i.e. the larger the coefficient, the

488 greater the effect of that term. The sign on the coefficient suggests the direction of the
489 effect (positive or negative).

490

491 The best-fitting equations of splash erosion rate for Fujian sand (Eq. 1) and sand/silt
492 mixture (Eq. 2) are in the form:

493 (1)

494 (2)

495 where E_s denotes splash erosion rate. The fitting equations of average sediment
496 concentration are obtained for Fujian sand and sand/silt mixture in Eq. 3 and 4 as
497 follows:

498 (3)

499 (4)

500 where S_a denotes average sediment concentration. The peak sediment concentration
501 for Fujian sand and sand/silt mixture were described by the Eq. 5 and 6 respectively:

502 (5)

503 (6)

504 where S_p denotes peak sediment concentration, and the signs of coefficients of
505 were opposite between Fujian sand and sand/silt mixture. The time to peak sediment
506 is fitted by CA and rainfall intensity in the form below (Eq. 7 for Fujian sand and Eq. 8
507 for sand/silt mixture):

508 (7)

509 (8)

510 where T_p denotes time to peak sediment. The correlation matrix of the Pearson
511 correlation coefficients for CA, rainfall intensity and erosional variables was displayed
512 in Table 3.

513

514 **5. Discussion**

515

516 *5.1. Effect of soil water repellency*

517

518 Soil water repellency has been found to promote splash erosion and accelerate
519 surface erosion. Splash erosion rate showed a significant increase with the water
520 repellency level (Fig. 8), from 0.01-0.10 g/mm (wetable soils) to 0.12-0.41 g/mm
521 (water repellent soils), as suggested by Eq. 1-2. The results were in accordance with
522 those previously reported in the literature (Fox et al., 2007; Ahn et al., 2013; Jordán et
523 al., 2016) with water repellent soils exhibiting greater soil particle detachment caused

524 by rain splash, regardless of the origin of water repellency (naturally occurring or
525 chemically induced), grain size (coarse-grained or fine-grained), and raindrop
526 characteristics (single raindrop or simulated rainfall). The time to peak sediment was
527 sensitive to wettability change as it shortened with increased CA, from 20-120 min for
528 wettable soils to 4-60 min for water repellent soils (Fig. 7a and 7b). In addition, the
529 peak sediment concentration always occurred after the onset of surface runoff,
530 implying that concentrated overland flow is the dominant mechanism controlling
531 surface erosion.

532

533 *5.2. Interaction effect between soil water repellency and grain size*

534

535 An interaction effect between soil water repellency and grain size on sediment yield
536 was identified, demonstrated by the following two variables: average sediment
537 concentration and peak sediment concentration. Fig. 7c and 7d showed that the
538 average sediment concentration increased from wettable sand (0-47.75 g/L) to water
539 repellent sand (2.25-105.64 g/L), but decreased for sand/silt mixture, from
540 74.05-108.95 g/L for the wettable to 5.83-20.91 g/L for the water repellent. The
541 opposite signs of coefficients of β_1 between Eq. 3 and 4 indicate that the effect of
542 soil wettability differs for different grain sizes. The same trend was observed for the
543 peak sediment concentration (Fig. 7e and 7f), which increased from 0-75.78 g/L to
544 3.57-236.19 g/L for sand but declined from 160.81-302.95 g/L to 20.22-74.12 g/L for
545 sand/silt mixture (Eq. 5 and 6). The variation in results between Fujian sand and

546 sand/silt mixture may be attributed to different erosion mechanisms. For Fujian sand,
547 the concentrated overland flow is the dominant mechanism controlling erosion, which
548 is positively influenced by water repellency. For sand/silt mixture, erosion is controlled
549 by both overland flow and subsurface flow, as stated in Fox and Wilson (2010). When
550 soil water repellency is present, infiltration as well as the subsurface flow is inhibited,
551 leading to a reduction in sediment concentration. Similar results were also reported in
552 Larsen et al. (2009), where artificial rainfall was applied on both a granitic soil and a
553 micaceous soil collected from burned hillslopes (water repellent), and the influence of
554 water repellency was found to be sensitive to the soil type, with higher runoff
555 coefficient and lower sediment concentration observed on the granitic soil. Erosional
556 impacts of soil water repellency were also investigated in the field. Osborn et al. (1964)
557 compared soil loss on newly burnt, water repellent chaparral soils and plots treated
558 with wetting agents and documented that sediment yields on the untreated plots were
559 almost 14 times higher than on treated counterparts. Consistent conclusions were
560 drawn by applying simulated rainfall with clean water and surfactant-treated water (to
561 eliminate water repellency) on burned slopes (WDPT > 5 h), with the sediment yield
562 increasing by 23 times when water repellency was present (Leighton-Boyce et al.,
563 2007).

564

565 When comparing the sediment loss between sand and sand/silt mixture under water
566 repellent conditions, the average and peak sediment concentration of water repellent
567 sand was much greater (Fig. 7c-7f). It is speculated that this difference may result

568 from a contrasting surface topography, e.g. microtopographic roughness, where two
569 quite different flow regimes can be defined depending on the height of the roughness
570 elements (Fig. 10). Powell (2014) and Bryan (2000) proposed that for smooth surface
571 (sand/silt mixture), the roughness elements (silt particles) are entirely submerged by
572 the laminar sublayer and the erosive force is resisted by the complete bed surface,
573 such a flow is said to be hydraulically (or dynamically) smooth, with the boundary
574 Reynolds number < 3.5 . However, for a rough surface (Fujian sand), the
575 roughness elements (sand particles) penetrate the laminar sublayer, causing a
576 hydraulically rough flow with the erosive force concentrated on and resisted by the
577 roughness elements, eventually leading to a greater soil erosion. The Pearson
578 correlation analysis (Table 3) also supported the statement that the impacts of water
579 repellency and rainfall intensity differ between Fujian sand and sand/silt mixture.

580

581 *5.3. Effect of grain size*

582

583 Fig. 9 summarizes the temporal change in sediment size distribution of sand and
584 sand/silt mixture separately and reveals that grain size plays an important role in the
585 size selectivity of sediment. The grain size distribution for sediment of Fujian sand
586 barely changes with time, whereas for sand/silt mixture, the collected sediment is
587 enriched with silt-sized particles at the beginning of experiments and gradually
588 becomes coarser, until the similar distribution as the original soil is approached. The
589 sediment size selectivity in flow-driven soil erosion processes was also observed by

590 Asadi et al. (2011), and two erosion mechanisms involved were explained.
591 Suspension-saltation (fine particles are carried by water flow or bounce along the
592 slope surface) is assumed to be the main erosion mechanism at the commencement
593 of experiments, only silt particles are affected. With the increase of runoff rate, a bed
594 load transport driven mechanism is suggested with coarse particles rolling on the
595 surface.

596

597 In addition, the effect of grain size on wettable soils agreed with Fox and Wilson (2010)
598 and Torfs et al. (2000). Average sediment concentration and peak sediment
599 concentration of sand/silt mixtures were much greater than those of Fujian sand,
600 which increased from 0-47.75 g/L to 74.05-108.95 g/L, and from 0-75.78 g/L to
601 160.81-302.95 g/L, respectively (Fig. 7c-7f). During the experiments of wettable
602 sand/silt mixture, subsurface flow was observed from the transparent flume sides,
603 which was a major contributor to the greater sediment yield. Subsurface flow can lead
604 to increased soil erosion on wettable soils through coupled mechanisms, including
605 hydraulic gradient forces that reduce the resistance of the particle to dislodgment from
606 the soil matrix and particle mobilization when soil particles are entrained in the
607 exfiltrating water.

608

609 *5.4. Effect of rainfall intensity*

610

611 Splash detachment has been reported to depend on the rainfall kinetic energy

612 (Nearing et al., 2017), which can be determined by the rainfall intensity and raindrop
613 size, and this conclusion is further supported by this study (the corresponding rainfall
614 kinetic energy of four rainfall intensities in this study are 235.2, 588.0, 999.6 and
615 1352.4 J/m²/h, respectively). Fig. 8 showed that the splash erosion rate increased
616 with rainfall intensity for the same wettability level, although soil water repellency has
617 a dominant impact on the splash erosion rate whereas rainfall intensity has only a
618 minor contribution. For rainfall to initiate erosion processes, thresholds of particle
619 detachment or transport need to be exceeded (Greene and Hairsine, 2004). This
620 study found that the erosion thresholds are influenced by soil water repellency and
621 grain size. Fig. 7c and 7e show that the sediment concentration of wettable Fujian
622 sand subjected to 40 mm/h rainfall is 0.0 g/L, while sediment was collected for the
623 water repellent sand at the same rainfall intensity. It is also noticed that the erosion
624 threshold of sand particles is greater than silt, considering that only silt is contained in
625 the sediment in test 23 (mixture, CA = 90°, rainfall intensity = 40 mm/h, Fig. 5a).
626 Sharma et al. (1991) also concluded that the threshold kinetic energy of raindrop
627 needed to initiate soil detachment is grain size dependent, with sandy and loam soil
628 reported to have a smaller threshold. Fig. 7c-7f also showed that with an increase in
629 rainfall intensity from 40 mm/h to 230 mm/h, higher average and peak sediment
630 concentrations were observed, with an exception of wettable sand/silt mixture (Fig. 7d
631 and 9f), implying the influence of rainfall intensity is minor compared with that of grain
632 size.

633

634 5.5. *Experimental considerations and implications*

635

636 The lower end of the flume was narrower than the upper part, to facilitate the
637 collection of eroded material. However, this set-up has caused concentrated flow and
638 greater soil erosion. In this study, surface runoff and subsurface flow were not
639 separated due to experimental constraints. As the impact of soil water repellency on
640 them might be different, it would be beneficial to collect the subsurface and overland
641 flows separately. In addition, a video camera was used to record the surface
642 morphology change in this study, which only provided qualitative information. To
643 quantitatively analyze the evolution in micro-topography of soil surface, terrestrial
644 laser scanner could be adopted.

645

646 Synthetic water repellent soils have been regarded as promising materials to be
647 utilized in the built environment as infiltration barriers, however the erosion yields of
648 these materials need to be controlled to guarantee a satisfactory performance. At this
649 stage and given the preliminary nature of this study, we cannot provide guidelines or
650 firm recommendations on their use. Our findings imply that infiltration can be reduced
651 in synthetic water repellent soils without amplifying erosion by taking grain size into
652 consideration. In particular, the results suggest that finer soils are more appropriate
653 because they are less prone to erosion while maintain water repellency, and therefore
654 reveal potential for use in the built environment.

655

656 **6. Conclusions**

657

658 Twenty-four flume tests under artificial rainfall at various soil wettability levels, grain
659 sizes and rainfall intensities were conducted to isolate and investigate the impact of
660 soil water repellency on soil erosion processes. The results reveal that: (1) soil water
661 repellency does not necessarily lead to increased soil erosion, its impact on erosion is
662 dependent on grain size and the erosion processes involved. (2) There is a
663 statistically significant positive correlation between splash erosion and soil water
664 repellency, indicating that greater rain splash can be expected on synthetic water
665 repellent soils, regardless of grain size. Higher rainfall kinetic energy also contributes
666 to promoted splash erosion, with relatively minor influence. (3) Particle size
667 distribution of eroded sediment is sensitive to grain size and insensitive to soil water
668 repellency. No variation in sediment particle size distribution is observed with the
669 Fujian sand, whereas the eroded sediment of sand/silt mixture gradually becomes
670 coarser until reaching a similar distribution to the original soil. These findings imply
671 that infiltration can be reduced in synthetic water repellent soils without amplifying
672 erosion by taking grain size into consideration.

673

674 **Acknowledgments**

675

676 This research is financially supported by the Research Grants Council of Hong Kong
677 (grant No. 17205915 and T22-603/15-N). Laboratory assistance by Mr. N. C. Poon

678 and Mr. Jiejia Yao is acknowledged.

679 **References**

680

681 Afshar, F. A., Ayoubi, S., & Jalalian, A. (2010). Soil redistribution rate and its
682 relationship with soil organic carbon and total nitrogen using ¹³⁷Cs technique in
683 a cultivated complex hillslope in western Iran. *Journal of Environmental*
684 *Radioactivity*, 101(8), 606-614.

685 Ahn, S., Doerr, S. H., Douglas, P., Bryant, R., Hamlett, C. A. E., McHale, G., . . .

686 Shirtcliffe, N. J. (2013). Effects of hydrophobicity on splash erosion of model soil
687 particles by a single water drop impact. *Earth Surface Processes and Landforms*,
688 38(11), 1225-1233.

689 Asadi, H., Moussavi, A., Ghadiri, H., & Rose, C. W. (2011). Flow-driven soil erosion
690 processes and the size selectivity of sediment. *Journal of Hydrology*, 406(1),
691 73-81.

692 Atherton, S., Polak, D., Hamlett, C. A. E., Shirtcliffe, N. J., McHale, G., Ahn, S., . . .

693 Newton, M. I. (2016). Drop impact behaviour on alternately hydrophobic and
694 hydrophilic layered bead packs. *Chemical Engineering Research and Design*,
695 110, 200-208.

696 Ayoubi, S., Ahmadi, M., Abdi, M. R., & Afshar, F. A. (2012). Relationships of ¹³⁷Cs
697 inventory with magnetic measures of calcareous soils of hilly region in
698 Iran. *Journal of Environmental Radioactivity*, 112, 45-51.

699 Ayoubi, S., Mokhtari, J., Mosaddeghi, M. R., & Zeraatpisheh, M. (2018a). Erodibility of
700 calcareous soils as influenced by land use and intrinsic soil properties in a

701 semiarid region of central Iran. *Environmental Monitoring and*
702 *Assessment*, 190(4), 192.

703 Ayoubi, S., Jabbari, M., & Khademi, H. (2018b). Multiple linear modeling between soil
704 properties, magnetic susceptibility and heavy metals in various land
705 uses. *Modeling Earth Systems and Environment*, 4(2), 579-589.

706 Bachmann, J., Ellies, A., & Hartge, K. (2000). Development and application of a new
707 sessile drop contact angle method to assess soil water repellency. *Journal of*
708 *Hydrology*, 231, 66-75.

709 Bisdom, E.B.A., Dekker, L.W., & Schoute, J. F. T. (1993). Water repellency of sieve
710 fractions from sandy soils and relationships with organic material and soil
711 structure. *Geoderma*, 56, 105-118.

712 Bryan, R. B. (2000). Soil erodibility and processes of water erosion on hillslope.
713 *Geomorphology*, 32(3-4), 385-415.

714 Bryan, R.B., & Poesen, J.W.A. (1989). Laboratory experiments on the influence of
715 slope length on runoff, percolation and rill development. *Earth Surface Processes*
716 *Landforms* 14, 211-231.

717 British Standards Institution. (1990). BS 1377:1990. Methods of test for soils for civil
718 engineering purposes.

719 Carollo, F. G., Ferro, V., & Serio, M. A. (2017). Reliability of rainfall kinetic
720 power-intensity relationships. *Hydrological Processes*, 31(6), 1293-1300.

721 Cerdà, A., Schnabel, S., Ceballos, A., & Gomez-Amelia, D. (1998). Soil hydrological
722 response under simulated rainfall in the Dehesa land system (Extremadura, SW

723 Spain) under drought conditions. *Earth Surface Processes and Landforms*, 23(3),
724 195-209.

725 Dell'Avanzi, E., Guizelini, A., da Silva, W., & Nocko, L. (2010). Potential use of
726 induced soil-water repellency techniques to improve the performance of landfill's
727 alternative final cover systems. *Unsaturated soils*. CRC Press, Boca Raton, FL,
728 461-466.

729 Doerr, S. H. (1998). On standardizing the 'water drop penetration time' and the
730 'molarity of an ethanol droplet' techniques to classify soil hydrophobicity: a case
731 study using medium textured soils. *Earth Surface Processes and Landforms*,
732 23(7), 663-668.

733 Doerr, S. H., Shakesby, R. A., Blake, W. H., Chafer, C. J., Humphreys, G. S., &
734 Wallbrink, P. J. (2006). Effects of differing wildfire severities on soil wettability and
735 implications for hydrological response. *Journal of Hydrology*, 319(1-4), 295-311.

736 Ebel, B. A., & Moody, J. A. (2017). Synthesis of soil-hydraulic properties and
737 infiltration timescales in wildfire-affected soils. *Hydrological Processes*, 31(2),
738 324-340.

739 Fox, G. A., & Wilson, G. V. (2010). The role of subsurface flow in hillslope and stream
740 bank erosion: A review. *Soil Science Society of America Journal*, 74(3), 717-733.

741 Fox, D. M., Darboux, F., & Carrega, P. (2007). Effects of fire-induced water repellency
742 on soil aggregate stability, splash erosion, and saturated hydraulic conductivity for
743 different size fractions. *Hydrological Processes*, 21(17), 2377-2384.

744 Greene, R. S. B., & Hairsine, P. B. (2004). Elementary processes of soil-water
745 interaction and thresholds in soil surface dynamics: A review. *Earth Surface*
746 *Processes and Landforms*, 29(9), 1077-1091.

747 Jordán, A., Zavala, L. M., Granged, A. J. P., Gordillo-Rivero, Á. J., García-Moreno, J.,
748 Pereira, P., . . . Alanís, N. (2016). Wettability of ash conditions splash erosion and
749 runoff rates in the post-fire. *Science of The Total Environment*, 572, 1261-1268.

750 Knapen, A., Poesen, J., Govers, G., Gyssels, G., & Nachtergaele, J. (2007).
751 Resistance of soils to concentrated flow erosion: A review. *Earth-Science*
752 *Reviews*, 80(1), 75-109.

753 Larsen, I. J., MacDonald, L. H., Brown, E., Rough, D., Welsh, M. J., Pietraszek, J.
754 H., . . . Schaffrath, K. (2009). Causes of post-fire runoff and erosion: Water
755 repellency, cover, or soil sealing? *Soil Science Society of America Journal*, 73(4),
756 1393-1407.

757 Leelamanie, D., Karube, J., & Yoshida, A. (2008). Characterizing water repellency
758 indices: Contact angle and water drop penetration time of hydrophobized sand.
759 *Soil Science & Plant Nutrition*, 54(2), 179-187.

760 Leighton-Boyce, G., Doerr, S. H., Shakesby, R. A., & Walsh, R. P. D. (2007).
761 Quantifying the impact of soil water repellency on overland flow generation and
762 erosion: A new approach using rainfall simulation and wetting agent on in situ soil.
763 *Hydrological Processes*, 21(17), 2337-2345.

764 Lourenço, S. D. N., Saulick, Y., Zheng, S., Kang, H., Liu, D., Lin, H., & Yao, T. (2018).
765 Soil wettability in ground engineering: fundamentals, methods, and applications.

766 Acta Geotechnica, 13(1), 1-14.

767 Mao, J., Nierop, K. G. J., Dekker, S. C., Dekker, L. W., & Chen, B. (2019).
768 Understanding the mechanisms of soil water repellency from nanoscale to
769 ecosystem scale: a review. *Journal of Soils and Sediments*, 19(1), 171-185.

770 McHale, G., Shirtcliffe, N. J., Newton, M. I., & Pyatt, F. B. (2007). Implications of ideas
771 on super-hydrophobicity for water repellent soil. *Hydrological Processes*, 21(17),
772 2229-2238.

773 Mohammadi, S., Homaei, M., & Sadeghi, S. H. (2018). Runoff and sediment behavior
774 from soil plots contaminated with kerosene and gasoil. *Soil and Tillage Research*,
775 182, 1-9.

776 Nearing, M. A., Yin, S.-q., Borrelli, P., & Polyakov, V. O. (2017). Rainfall erosivity: An
777 historical review. *Catena*, 157, 357-362.

778 Ng, S. H. Y., & Lourenço, S. D. N. (2016). Conditions to induce water repellency in
779 soils with dimethyldichlorosilane. *Géotechnique*, 66(5), 441-444.

780 Osborn, J.R., Pelishek, R.E., Krammes, J.S., & Letey, J. (1964). Soil wettability as a
781 factor in erodibility. *Soil Science Society of America Proceedings*, 28(2), 294–295.

782 Powell, D. M. (2014). Flow resistance in gravel-bed rivers: Progress in research.
783 *Earth-Science Reviews*, 136, 301-338.

784 Rahimi, M. R., Ayoubi, S., & Abdi, M. R. (2013). Magnetic susceptibility and Cs-137
785 inventory variability as influenced by land use change and slope positions in a
786 hilly, semiarid region of west-central Iran. *Journal of Applied Geophysics*, 89,
787 68-75.

788 Renard, K. G., Foster, G. R., Weesies, G. A., & Porter, J. P. (1991). RUSLE: Revised
789 universal soil loss equation. *Journal of Soil and Water Conservation*, 46(1), 30-33.

790 Saulick, Y., Lourenço, S. D. N., & Baudet, B. A. (2017). A semi-automated technique
791 for repeatable and reproducible contact angle measurements in granular
792 materials using the sessile drop method. *Soil Science Society of America Journal*,
793 81(2), 241-249.

794 Saulick, Y., Lourenço, S. D. N., Baudet, B. A., Woche, S. K., & Bachmann, J. (2018).
795 Physical properties controlling water repellency in synthesized granular solids.
796 *European Journal of Soil Science*, 69(4), 698-709.

797 Shakesby, R. A., Coelho, C. D. O. A., Ferreira, A. D., Terry, J. P., & Walsh, R. P. (1993).
798 Wildfire impacts on soil erosion and hydrology in wet Mediterranean forest,
799 Portugal. *International Journal of Wildland Fire*, 3(2), 95-110.

800 Sharma, P. P., Gupta, S. C., & Rawls, W. J. (1991). Soil detachment by single
801 raindrops of varying kinetic energy. *Soil Science Society of America Journal*,
802 55(2), 301-307.

803 Sheridan, G.J., So, H.B., Loch, R.J., Pocknee, C., & Walker, C.M. (2000). Use of
804 laboratory-scale rill and interrill erodibility measurements for the prediction of
805 hillslope-scale erosion on rehabilitated coal mine soils and overburdens.
806 *Australian Journal of Soil Research* 38, 285–297.

807 Sheridan, G. J., Lane, P. N. J., & Noske, P. J. (2007). Quantification of hillslope runoff
808 and erosion processes before and after wildfire in a wet Eucalyptus forest.
809 *Journal of Hydrology*, 343(1–2), 12-28.

810 Shi, P., Arter, C., Liu, X., Keller, M., & Schulin, R. (2017). Soil aggregate stability and
811 size-selective sediment transport with surface runoff as affected by organic
812 residue amendment. *Science of The Total Environment*, 607-608, 95-102.

813 Tajik, S., Ayoubi, S., & Nourbakhsh, F. (2012). Prediction of soil enzymes activity by
814 digital terrain analysis: comparing artificial neural network and multiple linear
815 regression models. *Environmental Engineering Science*, 29(8), 798-806.

816 Tarchitzky, J., Lerner, O., Shani, U., Arye, G., Lowengart-Aycicegi, A., Brener, A., &
817 Chen, Y. (2007). Water distribution pattern in treated wastewater irrigated soils:
818 Hydrophobicity effect. *European Journal of Soil Science*, 58(3), 573-588.

819 Terry, J. P., & Shakesby, R. A. (1993). Soil hydrophobicity effects on rainsplash:
820 Simulated rainfall and photographic evidence. *Earth Surface Processes and
821 Landforms*, 18(6), 519-525.

822 Torfs, H., Jiang, J., & Mehta, A. J. (2000). Assessment of the erodibility of fine/coarse
823 sediment mixtures. In W. H. McAnally & A. J. Mehta (Eds.), *Proceedings in
824 Marine Science* (Vol. 3, pp. 109-123): Elsevier.

825 van Dijk, A. I. J. M., Bruijnzeel, L. A., & Rosewell, C. J. (2002). Rainfall intensity -
826 kinetic energy relationships: a critical literature appraisal. *Journal of Hydrology*,
827 261(1), 1-23.

828 Wang, Z., Wu, L., & Wu, Q. (2000). Water-entry value as an alternative indicator of
829 soil water-repellency and wettability. *Journal of Hydrology*, 231, 76-83.

830 Wischmeier, W. H., & Mannering, J. (1969). Relation of soil properties to its erodibility.
831 *Soil Science Society of America Journal*, 33(1), 131-137.

- 832 Zaiontz, C. (2018). Real Statistics Using Excel. www.real-statistics.com (accessed on
833 11 September 2018).
- 834 Zheng, S., Lourenço, S. D. N., Cleall, P. J., Chui, T. F. M., Ng, A. K. Y., & Millis, S. W.
835 (2017). Hydrologic behavior of model slopes with synthetic water repellent soils.
836 Journal of Hydrology, 554, 582-599.

837 **Captions of figures and tables**

838

839 Table 1: Physical properties of Fujian sand and crushed silica.

840 Table 2: Summary of settings and results of flume test, where α denotes contact angle;

841 i denotes rainfall intensity; S_a denotes average sediment concentration; S_p

842 denotes peak sediment concentration; T_p denotes time to peak sediment; E_s

843 denotes splash erosion rate. Statistically significant differences between

844 experiments ($p < 0.05$) are denoted by superscript letters (a, b, c etc.), values with

845 the same superscript letters mean that no statistically significant differences were

846 observed for these experiments.

847 Table 3: Correlation matrix for contact angle, rainfall intensity and erosional variables

848 (Fujian sand and sand/silt mixture), where α denotes contact angle; i denotes

849 rainfall intensity; S_a denotes average sediment concentration; S_p denotes peak

850 sediment concentration; T_p denotes time to peak sediment.

851

852 Figure 1: Schematic illustration of flume dimension and instrumentation.

853 Figure 2: Time series data for wettable and subcritical water repellent sand (test 7). (a)

854 Runoff rate and sediment concentration. (b) Volumetric water content at various

855 locations. (c) Surface morphology evolution, where the surface morphology

856 features were outlined by dotted lines.

857 Figure 3: Time series data for water repellent sand (test 3). (a) Runoff rate and

858 sediment concentration. (b) Volumetric water content at various locations. (c)

859 Surface morphology evolution, where the surface morphology features were
860 outlined by dotted lines.

861 Figure 4: Time series data for wettable sand/silt mixture (test 16). (a) Runoff rate and
862 sediment concentration. (b) Volumetric water content at various locations. (c)
863 Surface morphology evolution, where the surface morphology features were
864 outlined by dotted lines.

865 Figure 5: Time series data for subcritical water repellent sand/silt mixture. (a) Runoff
866 rate and sediment concentration (test 23). (b) Volumetric water content at various
867 locations (test 23). (c) Surface morphology evolution (test 5), where the surface
868 morphology features were outlined by dotted lines.

869 Figure 6: Time series data for water repellent sand/silt mixture (test 6). (a) Runoff rate
870 and sediment concentration. (b) Volumetric water content at various locations. (c)
871 Surface morphology evolution, where the surface morphology features were
872 outlined by dotted lines.

873 Figure 7: Summary of erosional variables in flume tests: Time to peak sediment of (a)
874 sand and (b) sand/silt mixture; Average sediment concentration of (c) sand and (d)
875 sand/silt mixture; Peak sediment concentration of (e) sand and (f) sand/silt
876 mixture; Total mass of sediment of (g) sand and (h) sand/silt mixture; Time to
877 peak runoff of (i) sand and (j) sand/silt mixture.

878 Figure 8: Summary of splash erosion rate of (a) sand and (b) sand/silt mixture. The
879 ends of the box are the upper and lower quartiles, the median is marked by a
880 solid line inside the box, and the mean is marked by a cross inside the box, the

881 whiskers are the two lines outside the box that extend to the highest and lowest

882 values observed.

883 Figure 9: Summary of temporal change in D_{60} of sediment for (a) sand and (b)

884 sand/silt mixture.

885 Figure 10: Hydraulically smooth flow and rough flow on sand/silt mixture and Fujian

886 sand. *after* Powell (2014).

Figures and Tables

Properties	Fujian sand	crushed silica
Specific gravity, G_s	2.66	2.68
Maximum void ratio, e_{max}	0.56	1.74
Minimum void ratio, e_{min}	0.42	0.68
Coefficient of uniformity, C_u	5.56	2.80
Coefficient of curvature, C_c	0.34	0.86
Organic matter content, %	0.16	0.52

Table 1: Physical properties of untreated Fujian sand and crushed silica.

Test No.	Test settings			Test results			
	α (°)	Grain size	i (mm/h)	S_a (g/L)	S_p (g/L)	T_p (min)	E_s (g/mm)
1	20	Sand	230	47.75 ^{abc}	75.78 ^{abcd}	25 ^a	0.04 ± 0.01 ^{abc}
2	90			40.78 ^{abc}	89.67 ^{abcd}	15 ^a	0.03 ± 0.01 ^a
3	120			94.81 ^{abc}	236.19 ^{bcd}	5 ^a	0.29 ± 0.08 ⁱ
4	20	Mixture		74.05 ^{abc}	160.81 ^{abcd}	15 ^a	0.06 ± 0.02 ^{abcd}
5	90			28.45 ^{abc}	89.01 ^{abcd}	2 ^a	0.11 ± 0.03 ^{def}
6	120			20.91 ^{abc}	74.12 ^{abcd}	4 ^a	0.20 ± 0.02 ^{ij}
7	20	Sand	170	23.90 ^{abc}	48.17 ^{abc}	20 ^a	0.09 ± 0.02 ^{cde}
8	90			44.29 ^{abc}	119.28 ^{abcd}	10 ^a	0.12 ± 0.02 ^{defg}
9	120			105.64 ^{bc}	162.45 ^{abcd}	20 ^a	0.27 ± 0.03 ^{kl}
10	20	Mixture		80.63 ^{abc}	223.66 ^{abcd}	15 ^a	0.08 ± 0.01 ^{bcde}
11	90			15.20 ^{abc}	61.53 ^{abc}	2 ^a	0.13 ± 0.01 ^{efgh}
12	120			13.69 ^{abc}	55.30 ^{abc}	4 ^a	0.13 ± 0.01 ^{efgh}
13	20	Sand	100	9.78 ^{ab}	17.87 ^{ab}	65 ^{ab}	0.01 ± 0.01 ^a
14	90			1.41 ^a	6.30 ^{ab}	5 ^a	0.03 ± 0.01 ^a
15	120			12.08 ^{ab}	16.60 ^{ab}	5 ^a	0.15 ± 0.03 ^{fghi}
16	20	Mixture		108.95 ^c	261.11 ^{cd}	20 ^a	0.01 ± 0.00 ^a
17	90			7.60 ^{ab}	35.67 ^{abc}	5 ^a	0.04 ± 0.01 ^{abc}
18	120			5.83 ^a	37.81 ^{abc}	5 ^a	0.17 ± 0.02 ^{ghij}
19	20	Sand	40	0.00 ^a	0.00 ^a	120 ^b	0.02 ± 0.01 ^a
20	90			0.05 ^a	0.38 ^a	70 ^{ab}	0.04 ± 0.02 ^{abc}
21	120			2.25 ^a	3.57 ^{ab}	60 ^{ab}	0.22 ± 0.06 ^{jk}
22	20	Mixture		83.49 ^{abc}	302.95 ^d	30 ^a	0.01 ± 0.01 ^a
23	90			6.37 ^a	17.85 ^{ab}	15 ^a	0.05 ± 0.02 ^{abc}
24	120			6.58 ^{ab}	20.22 ^{ab}	15 ^a	0.19 ± 0.03 ^{hij}

Table 2: Summary of settings and results of flume test, where α denotes contact angle; i denotes rainfall intensity; S_a denotes average sediment concentration; S_p denotes peak sediment concentration; T_p denotes time to peak sediment; E_s denotes splash erosion rate. Statistically significant differences between experiments ($p < 0.05$) are denoted by superscript letters (a, b, c etc.), values with the same superscript letters mean that no statistically significant differences were observed for these experiments.

	Fujian sand					sand/silt mixture				
	α	i	S_a	S_p	T_p	α	i	S_a	S_p	T_p
α	1					1				
i	0	1				0	1			
S_a	0.333	0.748**	1			-0.929**	0.068	1		
S_p	0.357	0.770**	0.951**	1		-0.892**	-0.017	0.958**	1	
T_p	-0.45	-0.687*	-0.501	-0.528	1	-0.714**	-0.560	0.696*	0.739**	1

* Correlation is significant at $p < 0.05$ level

** Correlation is significant at $p < 0.01$ level

Table 3: Correlation matrix for contact angle, rainfall intensity and erosional variables (Fujian sand and sand/silt mixture), where α denotes contact angle; i denotes rainfall intensity; S_a denotes average sediment concentration; S_p denotes peak sediment concentration; T_p denotes time to peak sediment.

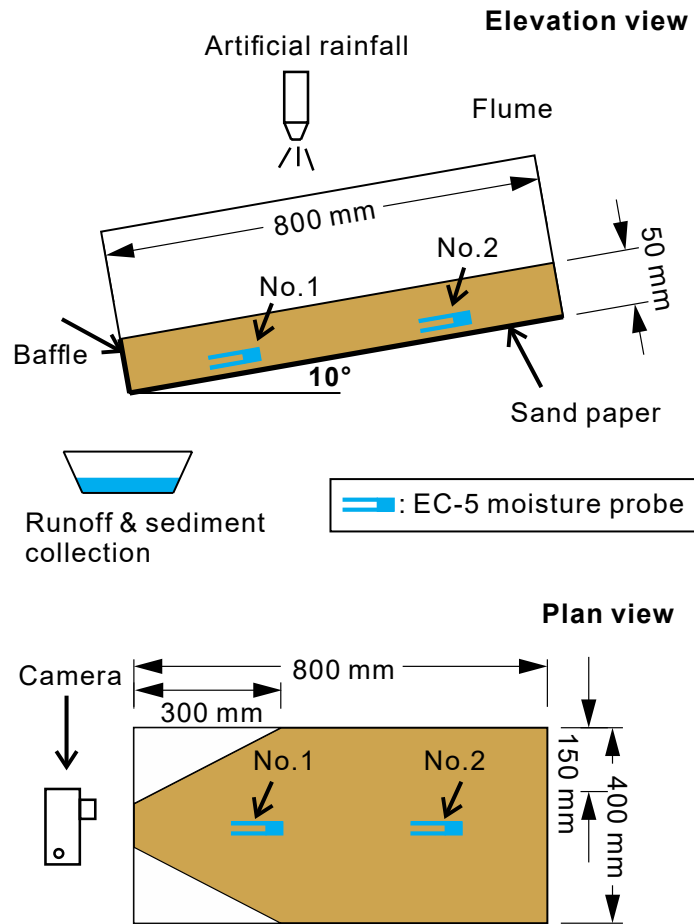


Figure 1: Schematic illustration of flume dimension and instrumentation.

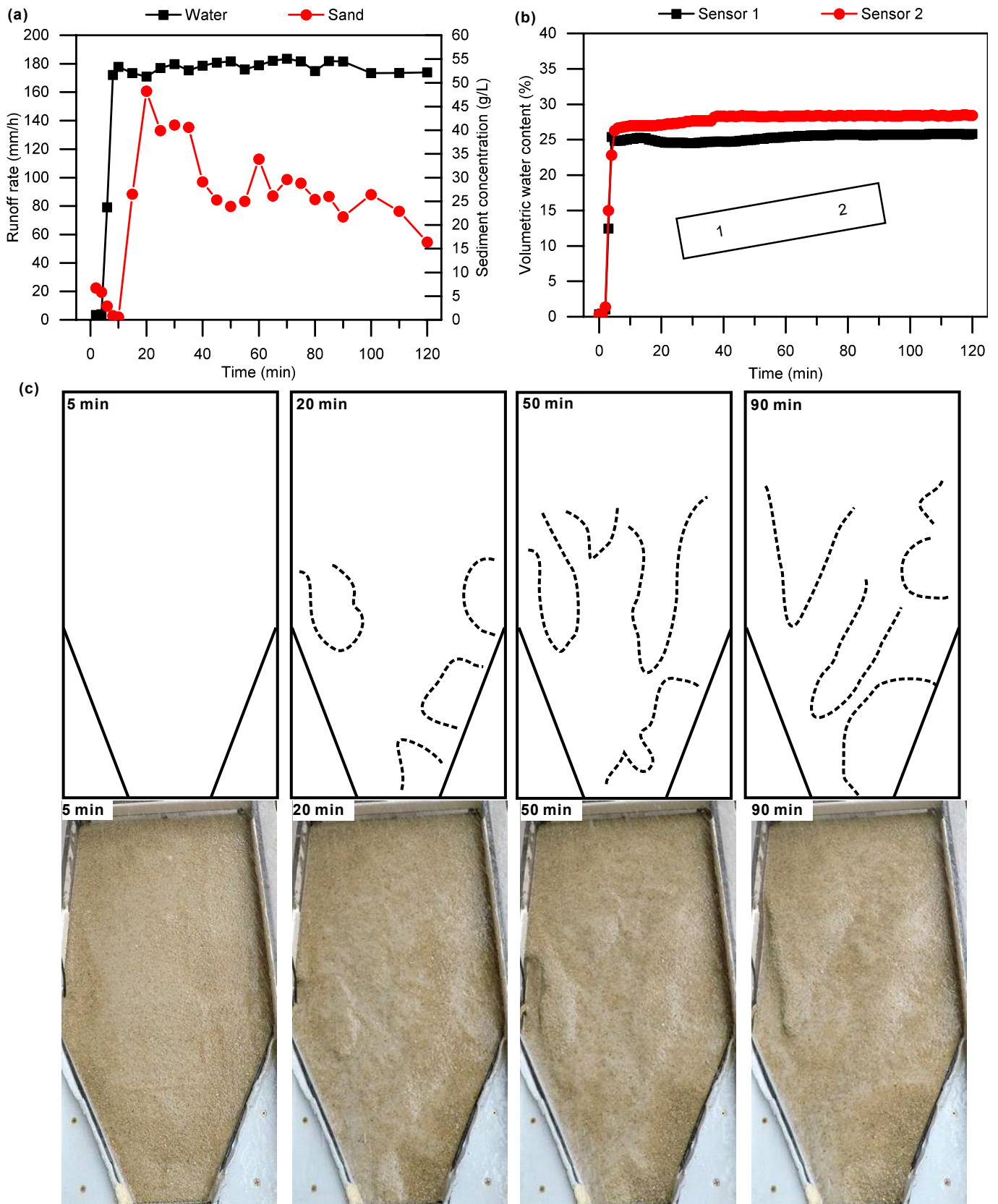


Figure 2: Time series data for wettable and subcritical water repellent sand (test 7). (a) Runoff rate and sediment concentration. (b) Volumetric water content at various locations. (c) Surface morphology evolution, where the surface morphology features were outlined by dotted lines.

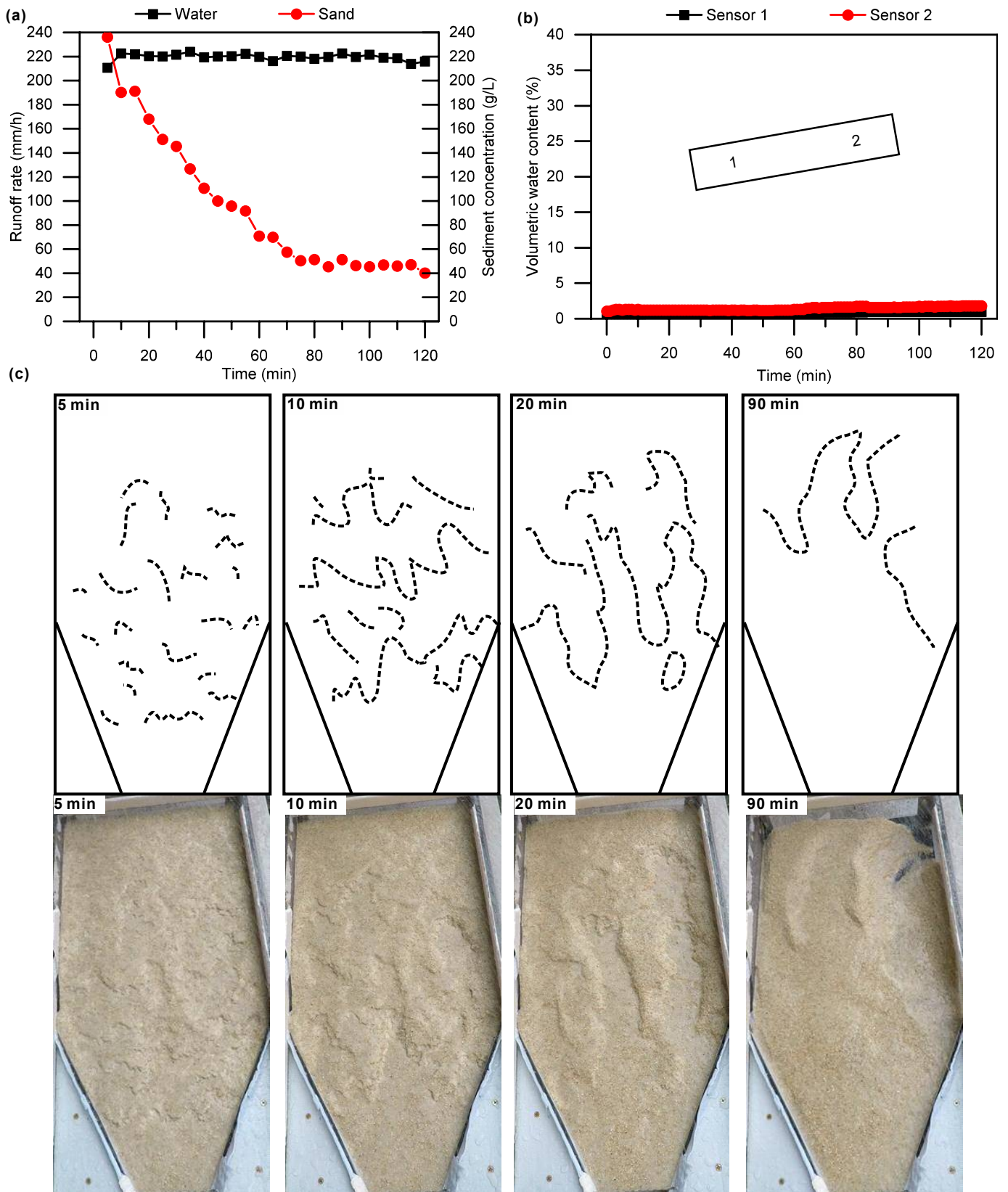


Figure 3: Time series data for water repellent sand (test 3). (a) Runoff rate and sediment concentration. (b) Volumetric water content at various locations. (c) Surface morphology evolution, where the surface morphology features were outlined by dotted lines.

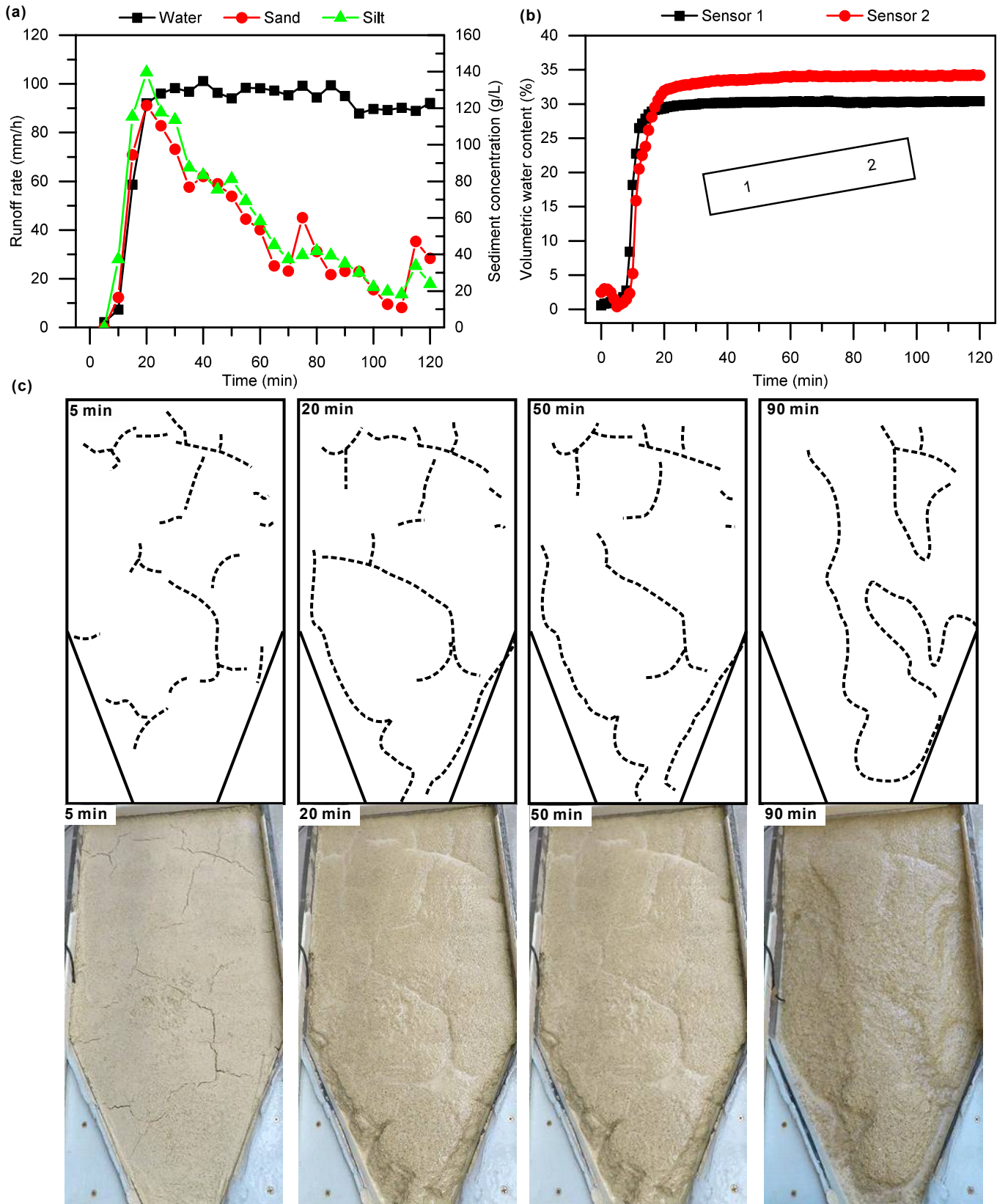


Figure 4: Time series data for wettable sand/silt mixture (test 16). (a) Runoff rate and sediment concentration. (b) Volumetric water content at various locations. (c) Surface morphology evolution, where the surface morphology features were outlined by dotted lines.

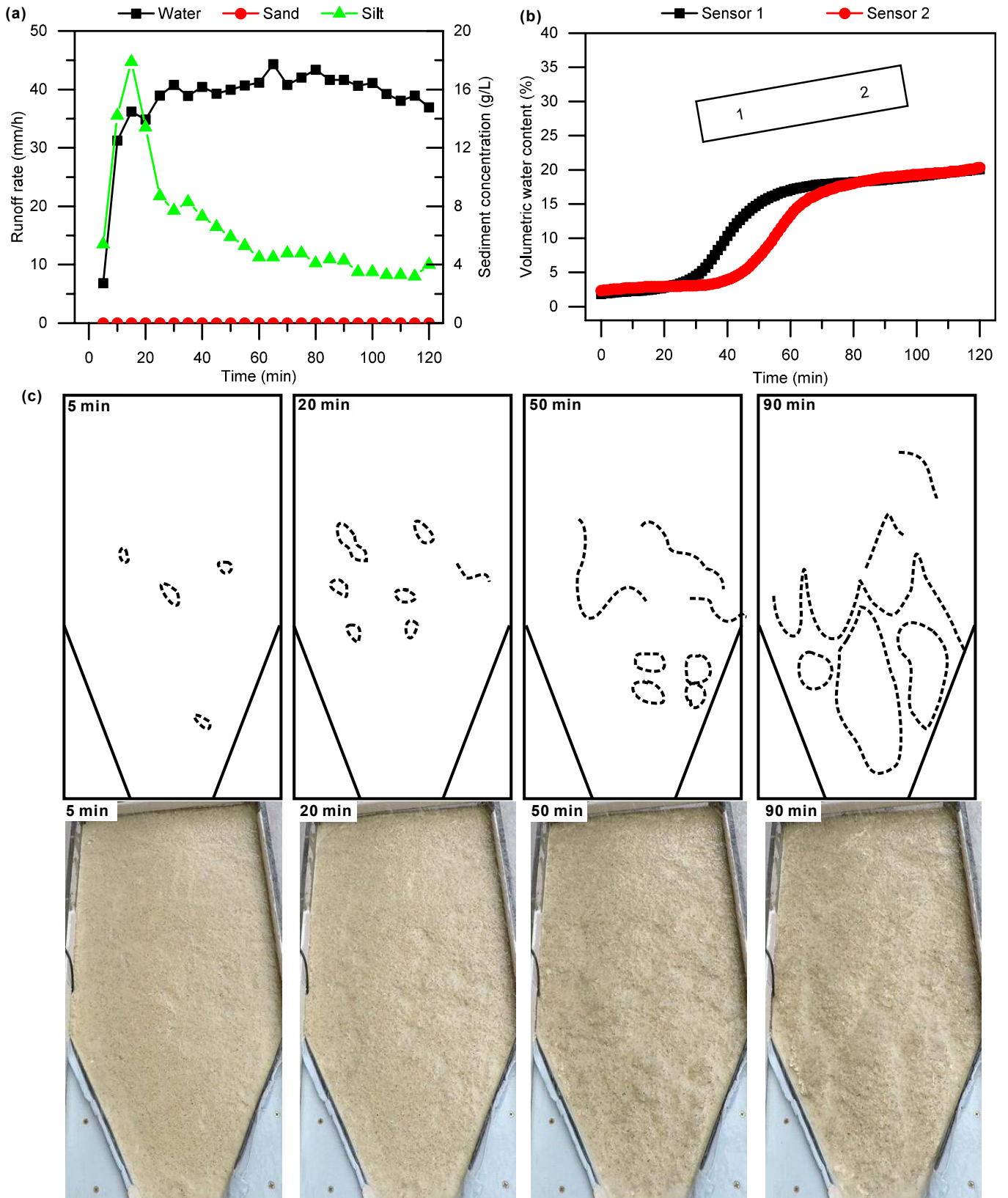


Figure 5: Time series data for subcritical water repellent sand/silt mixture. (a) Runoff rate and sediment concentration (test 23). (b) Volumetric water content at various locations (test 23). (c) Surface morphology evolution (test 5), where the surface morphology features were outlined by dotted lines.

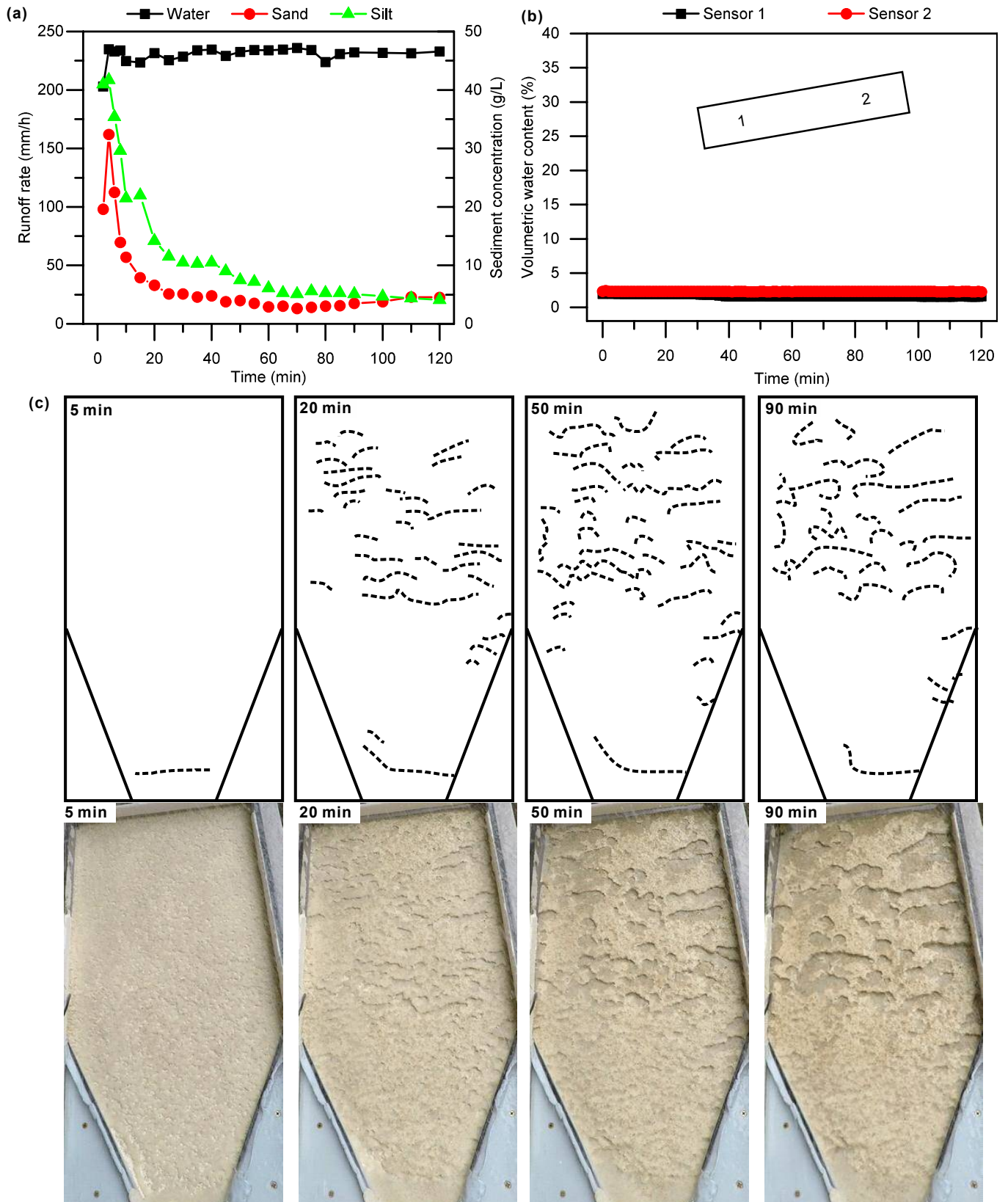


Figure 6: Time series data for water repellent sand/silt mixture (test 6). (a) Runoff rate and sediment concentration. (b) Volumetric water content at various locations. (c) Surface morphology evolution, where the surface morphology features were outlined by dotted lines.

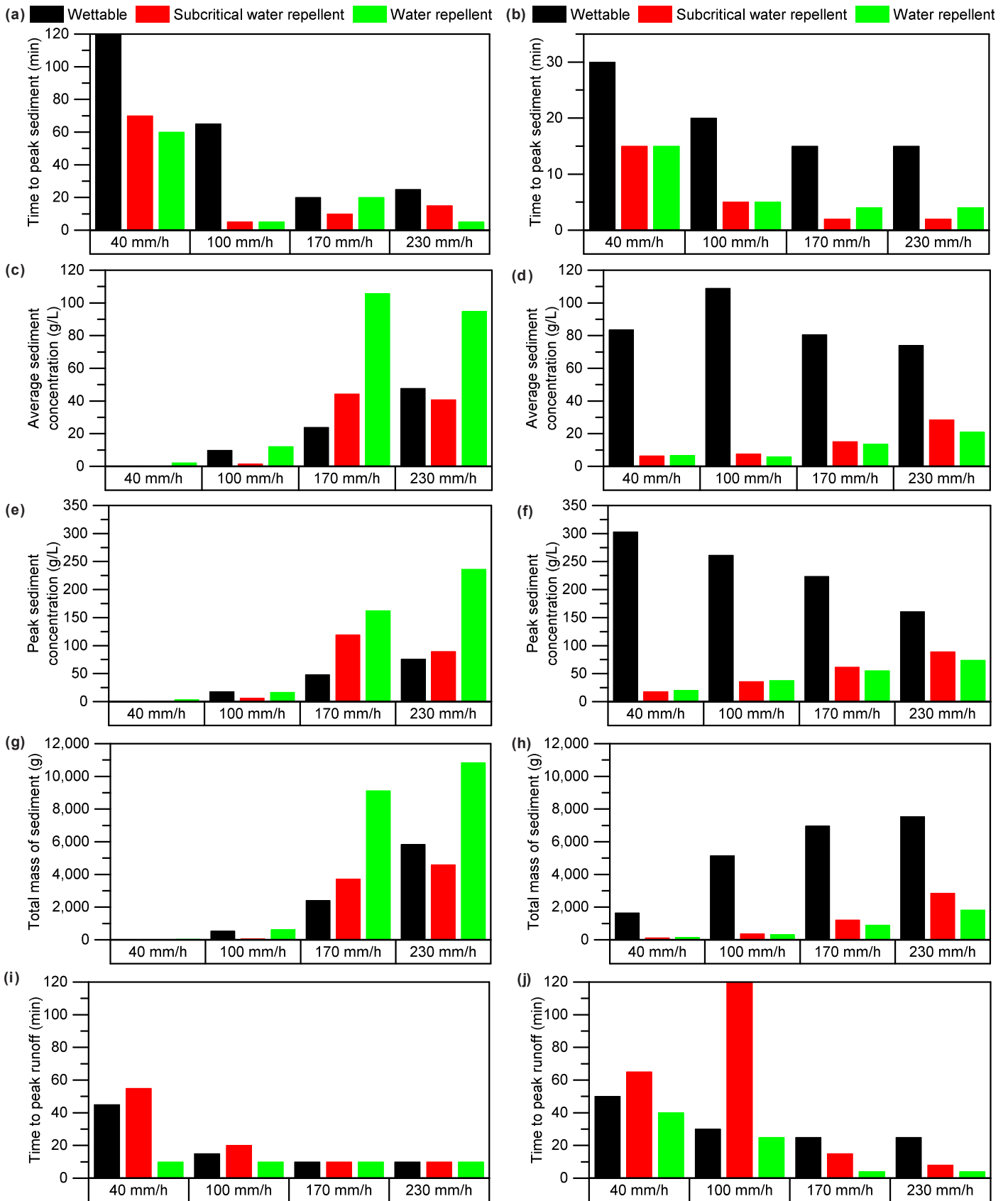


Figure 7: Summary of erosional variables in flume tests: Time to peak sediment of (a) sand and (b) sand/silt mixture; Average sediment concentration of (c) sand and (d) sand/silt mixture; Peak sediment concentration of (e) sand and (f) sand/silt mixture; Total mass of sediment of (g) sand and (h) sand/silt mixture; Time to peak runoff of (i) sand and (j) sand/silt mixture.

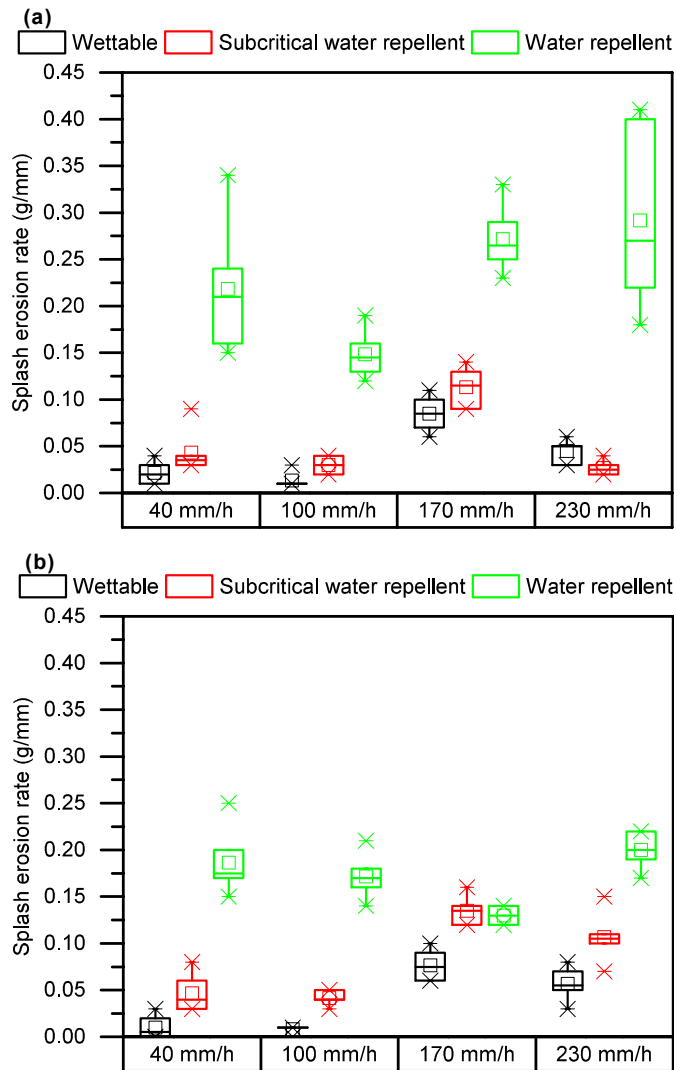


Figure 8: Summary of splash erosion rate of (a) sand and (b) sand/silt mixture. The ends of the box are the upper and lower quartiles, the median is marked by a solid line inside the box, and the mean is marked by a cross inside the box, the whiskers are the two lines outside the box that extend to the highest and lowest values observed.

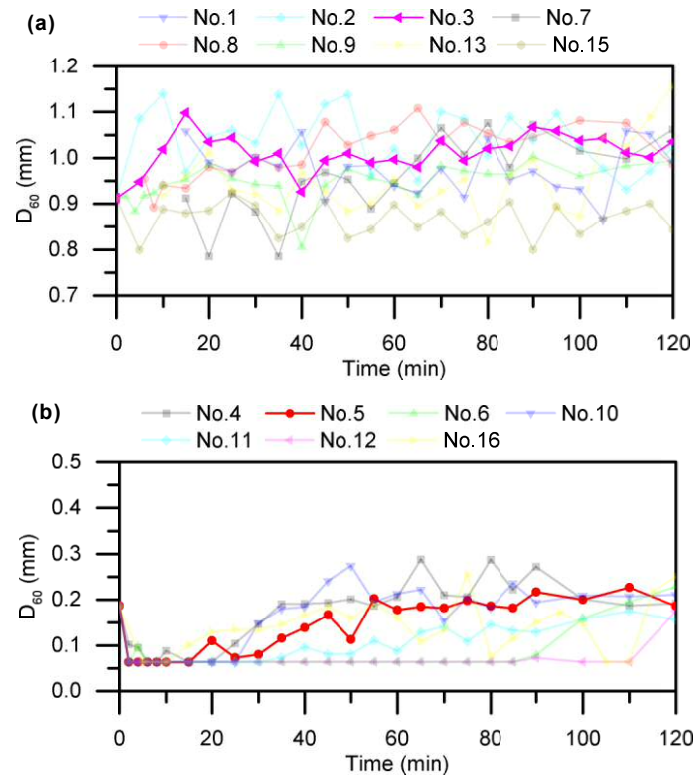


Figure 9: Summary of temporal change in D_{60} of sediment for (a) sand and (b) sand/silt mixture.

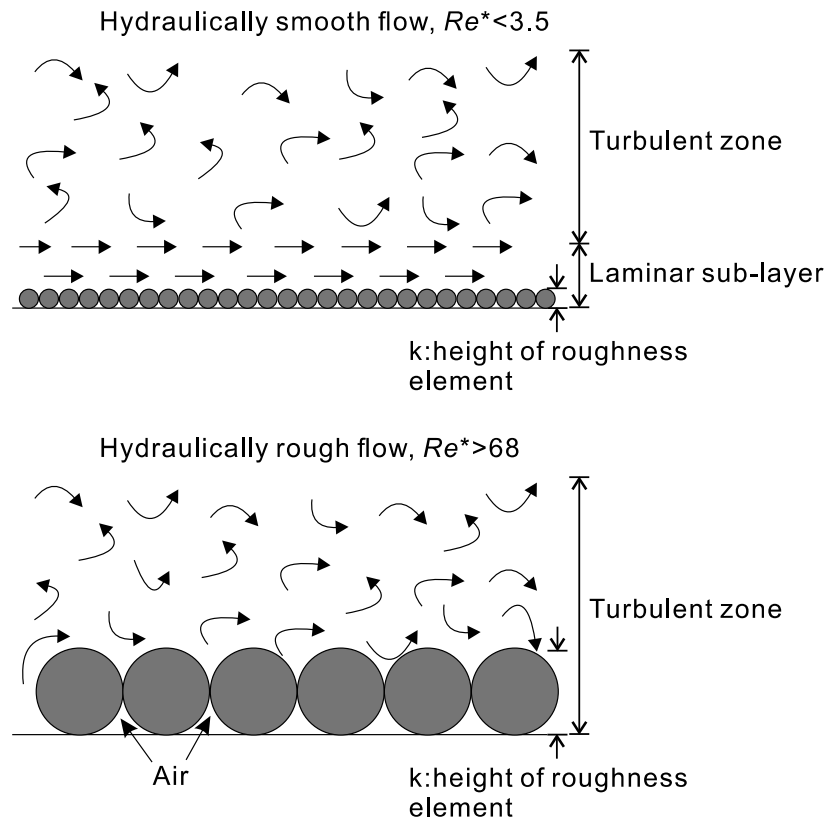


Figure 10: Hydraulically smooth flow and rough flow on sand/silt mixture and Fujian sand. *after* Powell (2014).

Supplementary materials:

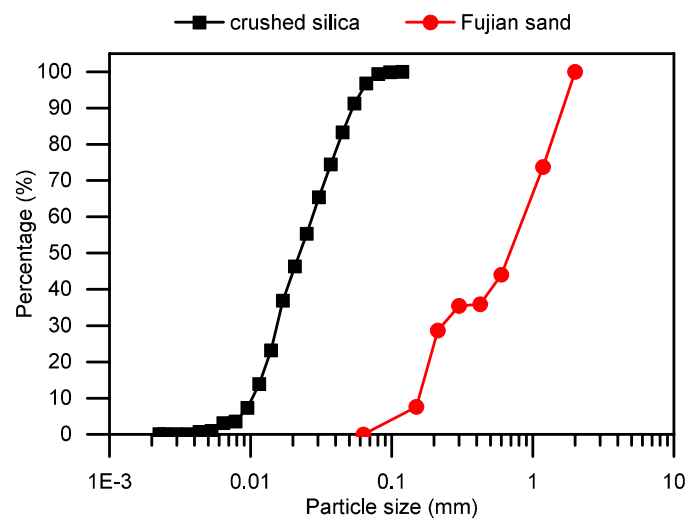


Figure S1: Particle size distributions of Fujian sand and crushed silica.

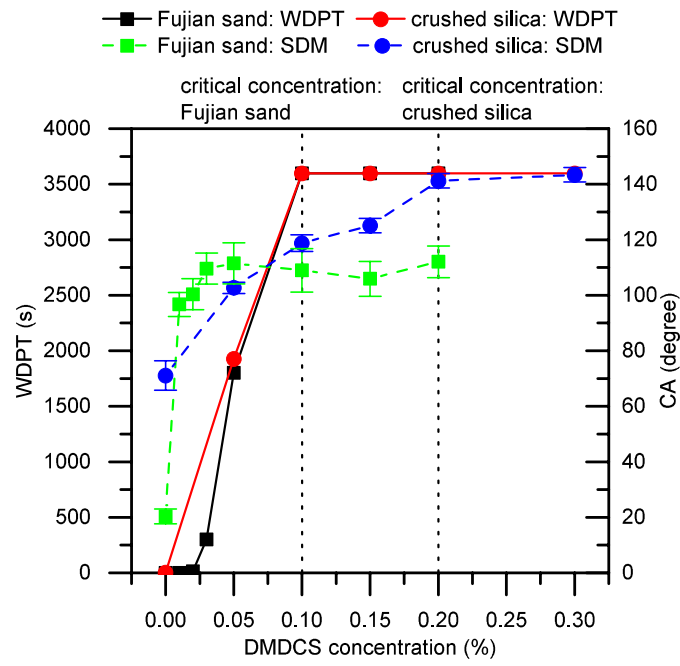


Figure S2: WDPT and CA for Fujian sand and crushed silica with various DMDCS concentration.